nature photonics

ARTICLES

https://doi.org/10.1038/s41566-020-00731-5

Ultrastrong plasmon–phonon coupling via epsilon-near-zero nanocavities

Daehan Yoo[1,7], Fernando de León-Pérez[2,3,7], Matthew Pelton[4], In-Ho Lee[1], Daniel A. Mohr[1], Markus B. Raschke[5], Joshua D. Caldwell[6], Luis Martín-Moreno[3]✉ and Sang-Hyun Oh[1]✉

Vibrational ultrastrong coupling, where the light–matter coupling strength is comparable to the vibrational frequency of molecules, presents new opportunities to probe the interactions between molecules and zero-point fluctuations, harness cavity-modified chemical reactions and develop novel devices in the mid-infrared spectral range. Here we use epsilon-near-zero nanocavities filled with a model polar medium (SiO_2) to demonstrate ultrastrong coupling between phonons and gap plasmons. We present classical and quantum-mechanical models to quantitatively describe the observed plasmon–phonon ultrastrong coupling phenomena and demonstrate a modal splitting of up to 50% of the resonant frequency (normalized coupling strength $\eta > 0.25$). Our wafer-scale nanocavity platform will enable a broad range of vibrational transitions to be harnessed for ultrastrong coupling applications.

The field of cavity quantum electrodynamics (QED) has generally divided light–matter interactions into two regimes: weak coupling, when losses exceed the light–matter coupling strength, and strong coupling, when the coupling strength dominates[1,2]. For weak-coupling phenomena such as the Purcell effect[3], Fano interference[4] and surface-enhanced infrared absorption[5], the coupled systems exchange energy on a timescale slower than the decay rates. In contrast, within the strong-coupling regime, the oscillators exchange their energy reversibly and coherently over an extended time frame that is longer than the decay rates[6–14], enabling applications such as quantum information processing[15]. Furthermore, strong coupling leads to the formation of hybridized energy states that are different from those of the bare constituents, leading to novel phenomena such as the modification of chemical reaction rates[2,16,17] and of ground-state reactivity[18].

Even more exotic phenomena can occur when the normalized coupling strength, η, of the system exceeds ~0.1, where η is defined as the ratio of the light–matter coupling strength, g, to the mid-gap frequency, ω. In this ultrastrong coupling (USC) regime[1,2,19,20], some of the standard approximations that are valid for weak coupling and strong coupling, such as the rotating-wave approximation, are expected to break down. Furthermore, transitioning from strong coupling to USC implies that the hybrid mode exhibits substantially more oscillations between light and matter states before decay, and such fast and efficient interactions can enable novel ultrafast devices[19,21]. Another striking phenomenon predicted in the USC regime, resulting from the antiresonant term in the light–matter coupling equation, is the possibility to extract virtual photons from the modified ground state via a dynamic Casimir effect[22,23]. Finally, USC between light and molecules has the potential to modify or enhance chemical reactions beyond what is possible in the strong-coupling regime[19].

Ultrastrong coupling has been demonstrated using photochromic molecules[24], circuit QED systems[25], intersubband polaritons[26], molecular liquids[27] and two-dimensional electron gases[28]. Strong coupling to vibrational modes at mid-infrared (MIR) frequencies has been demonstrated in various systems[18,29–32], enabling applications such as surface-enhanced vibrational spectroscopy[5,33], thermal emission and signature control, and modified heat transfer. It has been challenging, however, to achieve USC at MIR frequencies, particularly in solid-state systems, because of the relatively weak oscillator strengths for vibrational modes originating from lattice ionic motions. Previous demonstrations have involved extended microcavity structures[2,18,27], opening up a new physical regime at these technologically important frequencies, but with limited possibilities for novel nonlinear effects.

Here we demonstrate vibrational USC within nanocavities, drastically reducing the size of the system and thus the amount of material involved in achieving MIR USC. Specifically, we use coaxial nanocavities, which exhibit strong transmission resonances and field enhancements close to the cutoff frequency of the TE_{11}-like mode; these can be understood as resulting from excitation of the zeroth-order Fabry–Pérot resonance[34] or, alternatively, as arising from an effective epsilon-near-zero (ENZ) effect[35–37]. We couple this coaxial ENZ mode to the lattice vibrations of SiO_2 and demonstrate MIR USC with a mode splitting exceeding 50% of the vibrational transition frequency ($\eta > 0.25$) within a solid-state system.

Results

Design and fabrication of ENZ nanocavities. In our USC platform, SiO_2-filled coaxial nanoapertures fabricated into a metal (Au) film of thickness T are hexagonally arranged with varied gap size (G), diameter (D) and lattice periodicity (P) (Fig. 1a). Unlike conventional approaches of selectively etching annular gaps in metal films, we adopt a fabrication approach called atomic layer lithography[36,38] to create dielectric-filled nanogaps in metal films (Fig. 1c and Methods). After employing standard photolithography to define Au disk arrays on a silicon wafer, SiO_2 films are conformally grown via atomic layer deposition[38] (ALD) on the exposed surfaces

[1]Department of Electrical and Computer Engineering, University of Minnesota, Minneapolis, MN, USA. [2]Centro Universitario de la Defensa de Zaragoza, Zaragoza, Spain. [3]Instituto de Nanociencia y Materiales de Aragón (INMA) and Departamento de Física de la Materia Condensada, CSIC-Universidad de Zaragoza, Zaragoza, Spain. [4]Department of Physics, University of Maryland, Baltimore County, Baltimore, MD, USA. [5]Department of Physics and JILA, University of Colorado, Boulder, CO, USA. [6]Department of Mechanical Engineering, Vanderbilt University, Nashville, TN, USA. [7]These authors contributed equally: Daehan Yoo, Fernando de León-Pérez. ✉e-mail: lmm@unizar.es; sang@umn.edu

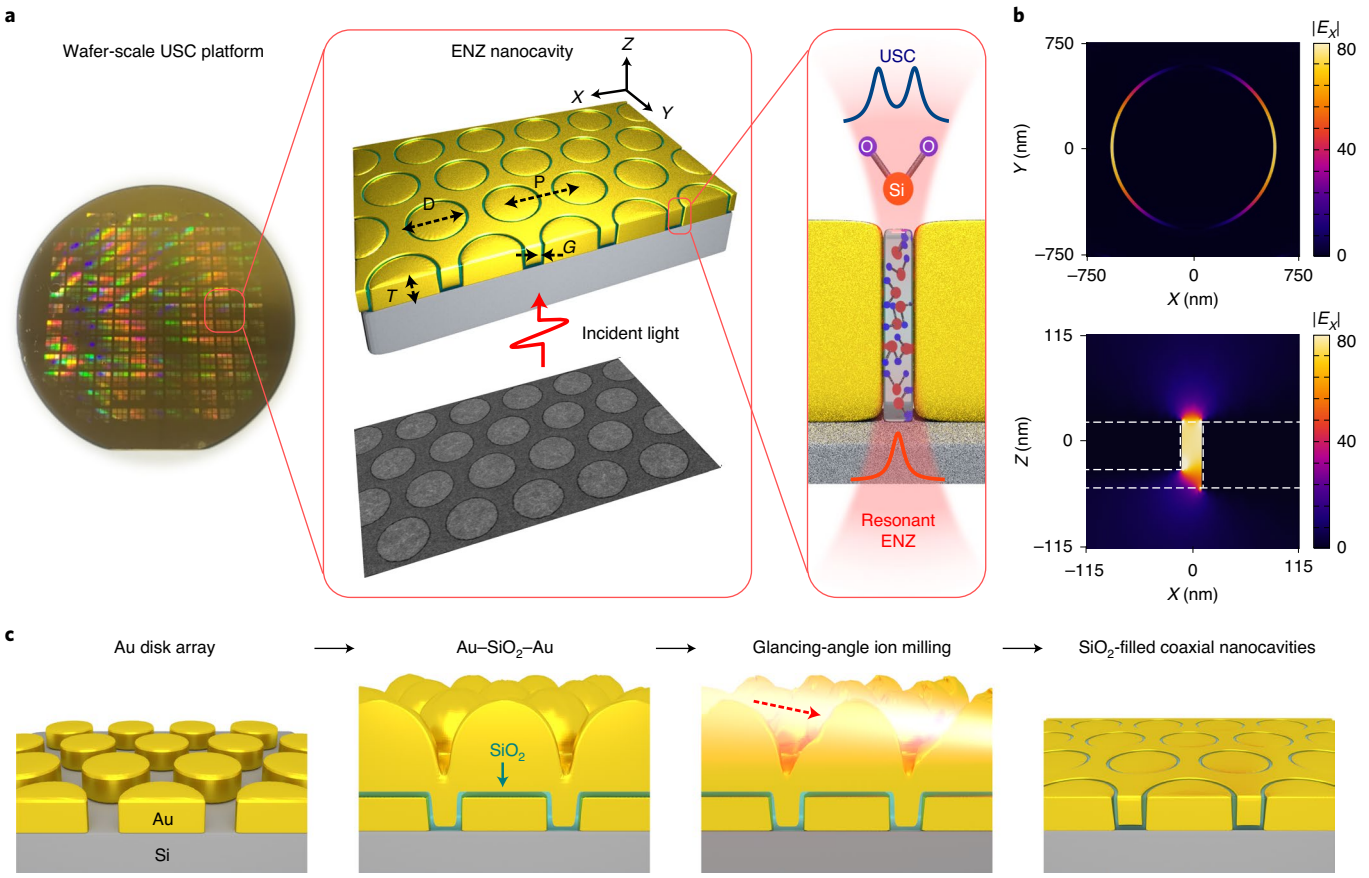

Fig. 1 | Wafer-scale resonant ENZ nanocavity platform for USC. a, Geometrical parameters and illustration of SiO_2 phonons interacting with the ENZ mode of the nanocavity. Inset: scanning electron micrograph of coaxial nanocavities with 21 nm gap, 790 nm diameter, 1,190 nm period and 80 nm Au thickness. **b**, Computed field profiles (for fields polarized in the lateral direction) of a coaxial nanocavity (diameter 1,120 nm and gap width 21 nm) showing a lateral section (upper) and a vertical section (lower) of the ENZ transmission resonance. The dashed white lines in the lower panel represent boundaries between different materials. **c**, Process flow based on ALD and wafer-scale glancing-angle ion milling. The dashed red arrow represents the direction of the glancing-angle ion beam.

and sidewalls, followed by subsequent metal cladding layer deposition and planarization via glancing-angle ion milling. This batch process can produce wafer-sized arrays of coaxial apertures with a gap size down to 1 nm, limited only by the ALD growth.

For very narrow gaps, TE_{11} coaxial modes have a strong plasmonic character. Such modes are characterized by an effective dielectric constant that is approximately zero at cutoff. The resonance frequency of the cavities can be shifted toward longer wavelengths without sacrificing modal confinement by increasing the coaxial diameter without changing the gap width. In addition, the very long wavelength associated with near-zero permittivity produces a spatially uniform optical field (Fig. 1b lower panel), which in turn provides efficient coupling to the material within the gaps.

We note that the ENZ resonance is a single-aperture effect; in other words, the existence of an array is not required for the transmission resonance we utilize (Supplementary Section 2). We also note that the resonant optical properties of the nanocavities are robust against process variations and inhomogeneous broadening for two reasons. First, the critical dimension (that is, the width of the nanogap) is lithography-independent and precisely defined by the thickness of the SiO_2 film grown by ALD. Second, the ENZ mode (that is, the zeroth-order Fabry–Pérot resonance) is independent of the cavity length, and is thus insensitive to variations in the Au film thickness.

We designed a series of cavities with diameters ranging from 430 nm to 1,120 nm in 30 nm steps, in order to tune the bare ENZ resonance from approximately 1,000 to 2,500 cm^{-1}. This range is chosen to cover the Reststrahlen band of SiO_2, which is defined by the transverse optical (TO) and longitudinal optical (LO) phonon frequencies (Fig. 2a). Coaxial nanocavities at the ENZ condition show extraordinary optical transmission (EOT)[39], since incident light with wavelengths 4–10 μm can pass through annular gaps that are over 1,000 times narrower than the wavelength, with the absolute transmittance as high as 60%.

Transmission spectra through the nanocavity arrays were measured by far-field Fourier transform infrared spectroscopy over a large-area (5 mm × 5 mm) chip containing arrays of coaxial nanocavities. The normalized transmission spectra for coaxial nanocavities filled with 21-nm-thick SiO_2 are plotted in Fig. 2b. The observed transmission features a clear anticrossing behaviour characteristic of strong coupling.

Although these results suggest that the SiO_2 phonons and cavity photons are strongly coupled, the split transmission peaks could potentially be interpreted as the result of a single broad transmission resonance being quenched in a central frequency range by the strong vibrational absorption close to ω_{TO}. To clarify the origin of the split transmission peaks, we perform a theoretical analysis of the coupled system to be compared to our experimental results.

Theoretical analysis of ultrastrong plasmon–phonon coupling. *Classical description.* Electromagnetic propagation in waveguides is usually based on a description where the phononic degrees of

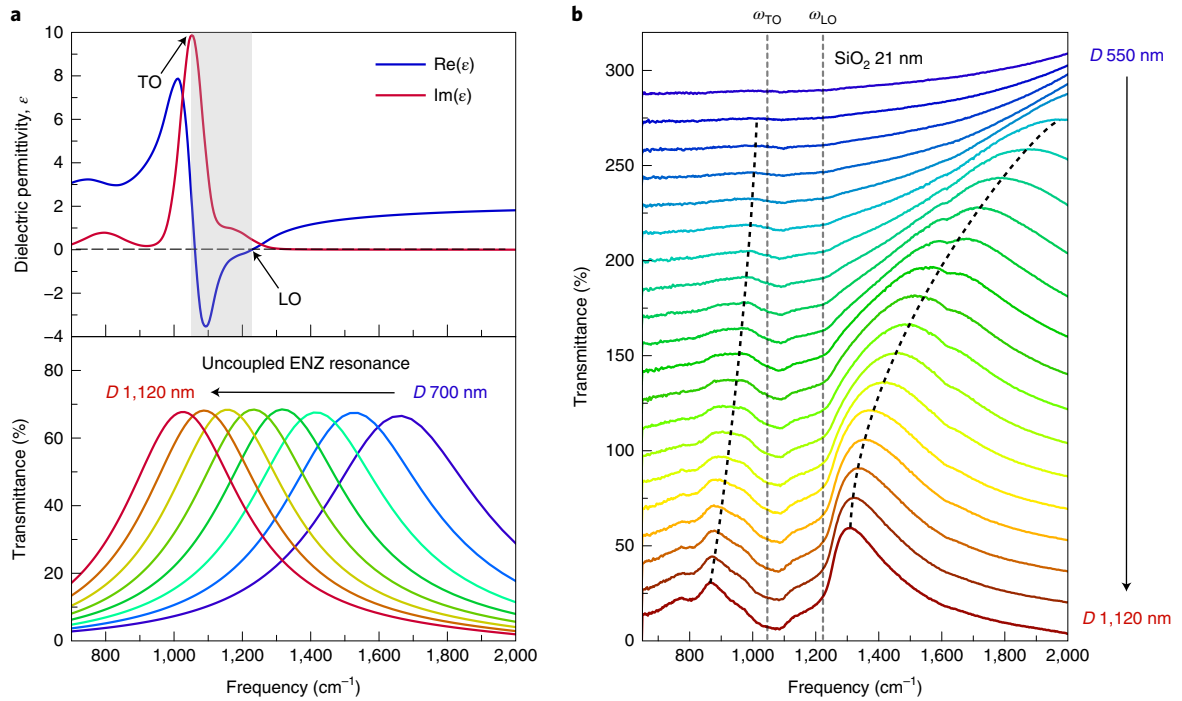

Fig. 2 | Normal mode splittings due to ultrastrong plasmon–phonon coupling. a, Dielectric function[50] of SiO_2 (upper) and ENZ transmission resonances (lower) of coaxial nanocavities (gap width of 21 nm, diameter from 700 nm to 1,120 nm), simulated with a frequency-independent dielectric constant ϵ_∞ inside the aperture. This calculation shows that the bare cavity resonance sweeps through the entire Reststrahlen band (grey region, upper panel) for the considered diameters (Supplementary Section 1). **b**, Normalized experimental transmission spectra of SiO_2-filled coaxial Au nanocavities, for gap width of 21 nm and diameter from 550 to 1,120 nm. Black dashed guidelines indicate the lower and upper polariton branches.

freedom have been integrated out, providing a frequency-dependent dielectric function $\epsilon(\omega)$ for the propagation of the photon (Supplementary Section 3). However, in order to determine whether the system is in the strong-coupling regime, it is essential to retain both phononic and photonic degrees of freedom. We therefore consider a given waveguide mode M, characterized by a wavevector k along the waveguide axis (in this case, $M = TE_{11}$, the fundamental mode of the coaxial waveguide). When the aperture is filled with a uniform dielectric constant ϵ_∞ (originating from coupling to electronic degrees of freedom), the electric field, $\mathbf{E}(\mathbf{r}) = E\mathbf{E}_M(\mathbf{r},k)$, where $\mathbf{r}$ is the vector position, satisfies the wave equation

$$\nabla\times\nabla\times E\mathbf{E}_M - \epsilon_\infty\frac{\omega_k^2}{c^2}E\mathbf{E}_M = 0, \quad (1)$$

where E is the field amplitude, $\mathbf{E}_M$ is a normalized transverse solution of Maxwell's equations (Supplementary Section 4) and c is the speed of light in vacuum. When the phononic material fills the waveguide, we assume a local relation (valid for non-dispersive vibrational modes) between $\mathbf{E}$ and the relative displacement of ions, $\mathbf{x}$, following ref. [40]. Then, for a given mode profile, $\mathbf{x}(\mathbf{r}) = x\mathbf{E}_M(\mathbf{r}, k)$, with

$$\ddot{x} = \gamma_{11}x + \gamma_{12}E, \quad (2)$$

$$P = \gamma_{12}x + \gamma_{22}E, \quad (3)$$

where P is the amplitude of polarization vector $\mathbf{P} = P\mathbf{E}_M$ and $\ddot{x}$ is the second derivative of x with respect to time. The phenomenological parameters γ_{ij} can be written in terms of measurable quantities: $\gamma_{12}^2 = \omega_p^2\epsilon_\infty/4\pi$ with $\omega_p^2 = \omega_{LO}^2 - \omega_{TO}^2$, $\gamma_{11} = -\omega_{TO}^2$ and $\gamma_{22} = (\epsilon_\infty - 1)/4\pi$ (Supplementary Section 3). Note that γ_{22} incorporates the effect of the electronic resonances excited at higher frequencies. The wave equation becomes, in this case

$$\nabla\times\nabla\times E\mathbf{E}_M - \frac{\omega^2}{c^2}(E + 4\pi P)\mathbf{E}_M = 0. \quad (4)$$

By inspection, we find that $\mathbf{E}_M(\mathbf{r}, k)$ satisfies equation (4) if $\omega^2(E + 4\pi P) = \epsilon_\infty\omega_k^2 E$ (strictly speaking, we are neglecting the variation between ω and ω_k in the impedance of the metal surrounding the waveguide; for a deeper analysis of how this affects the above condition, see Supplementary Sections 2 and 5). This condition, together with equations (2) and (3), can be expressed in a matrix form, stating that $\mathbf{E}_M(\mathbf{r}, k)$ is still a solution of Maxwell's equations but at a frequency ω satisfying

$$\begin{pmatrix} \omega^2 - \omega_{TO}^2 & \omega\,\omega_p \\ \omega\,\omega_p & \omega^2 - \omega_k^2 \end{pmatrix}\begin{pmatrix} \omega\,x \\ \sqrt{\epsilon_\infty/4\pi}E \end{pmatrix} = 0. \quad (5)$$

(See Supplementary Section 6 for a detailed derivation and a discussion of the effects of losses.) Note that the simpler coupled-harmonic-oscillator model that is commonly used for fitting experimental data (Supplementary Section 7) does not show the ω-dependence of the off-diagonal terms and therefore cannot describe the polaritonic branches correctly (Fig. 3a and Supplementary Fig. 6).

Quantum-mechanical description. We have used a classical approach above. For future work, especially the investigation of nonlinear optical effects, a full quantum-mechanical description will be required, wherein off-resonant terms may be important and the rotating-wave approximation cannot necessarily be applied[41–45].

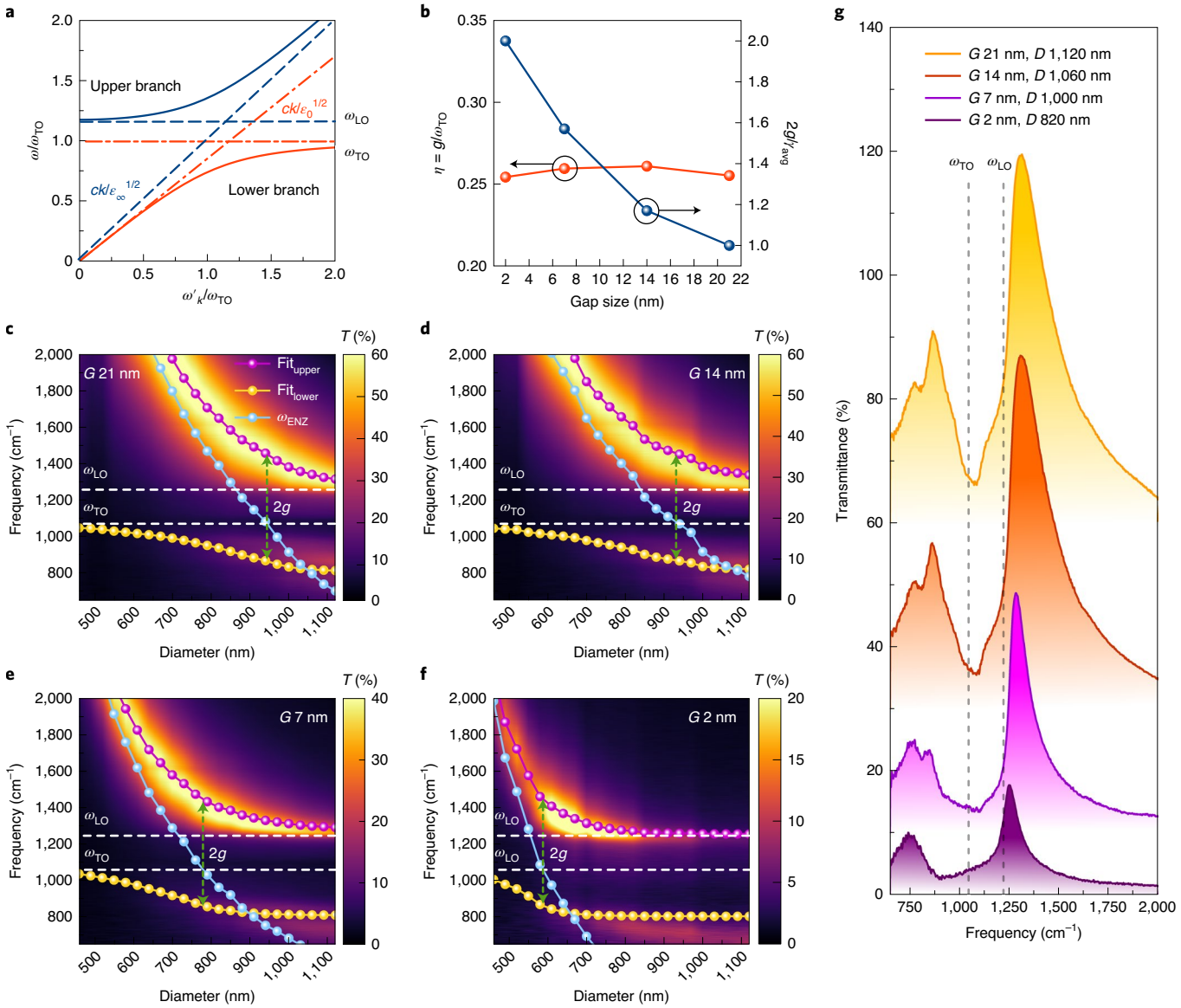

Fig. 3 | Dispersion mapping and validation of theoretical model. a, The dispersion relation of bulk phonon polaritons supported in SiO_2 as calculated by equation (5) under the assumption that a single vibrational mode is excited. **b**, The measured normalized coupling strength, η, and normalized mode splitting, $(2g/\gamma_{avg})$, as a function of gap size. **c**–**f**, Dispersion maps of experimentally measured transmission (T) spectra for coaxial apertures filled with SiO_2 with gap thicknesses of 21 nm (**c**), 14 nm (**d**), 7 nm (**e**) and 2 nm (**f**). Polaritonic resonances analytically fit using Supplementary equation (14) (purple (upper) and yellow (lower) circles and solid line). ω_{ENZ} (blue circles with solid line) is used as a fitting parameter and indicates the resonance of the ENZ mode uncoupled from the polar phonons of SiO_2. The coupling strength, g, is measured at the intersection between the uncoupled ENZ resonance and ω_{TO} (when the detuning is zero). **g**, Transmission spectra measured when the bare ENZ mode crosses through the Reststrahlen band, showing distinct modal splitting and sharp resonance peaks (60% transmittance for the 21-nm-wide coaxial gap). Curves are shifted along the vertical axis for clarity.

We therefore apply the canonical procedure of second quantization to the classical Hamiltonian (see Supplementary Section 9 for details). For the sake of convenience, absorption is neglected and the walls of the coaxial cavity are assumed to be perfectly conducting. We obtain a Hopfield-like Hamiltonian[41] for interacting photons and phonons: $H = H_{photon} + H_{phonon} + H_{int}$, with

$$H_{photon} = \sum_m \hbar\omega_m \left(a_m^+ a_m + \frac{1}{2}\right), \quad (6)$$

$$H_{phonon} = \sum_m \hbar\omega_{TO} \left(b_m^+ b_m + \frac{1}{2}\right), \quad (7)$$

$$H_{int} = \sum_m \hbar\left[iC_m\left(a_m^+ b_m - a_m b_m^+\right) + D_m\left(2a_k^+ a_m + 1\right) + iC_m\left(a_m b_m - a_m^+ b_m^+\right) + D_m\left(a_m a_m + a_m^+ a_m^+\right)\right]. \quad (8)$$

where $a^+(a)$ and $b^+(b)$ are the creation (annihilation) operators for photons and phonons, respectively, the sum is over modes m, and

$$C_m = \frac{\omega_p}{2}\sqrt{\frac{\omega_{TO}}{\omega_m}}, \quad D_m = \frac{\omega_p^2}{4\omega_m}. \quad (9)$$

As expected, given that the system comprises two coupled harmonic oscillators, diagonalizing the full Hamiltonian gives eigenfrequencies identical to those obtained from equation (5). In other

Table 1 | Mode splitting and normalized coupling strength

SiO_2 gap width (nm)	2	7	14	21
Bare ENZ mode linewidth (FWHM) (cm^{-1})	453	619	844	990
Average of bare ENZ and TO phonon linewidths, γ_{avg} (cm^{-1})	265	348	481	534
Normal mode splitting, $2g$ (cm^{-1})	534	546	549	537
Normalized mode splitting, $2g/\gamma_{avg}$	2.02	1.57	1.14	1.01
Normalized coupling strength, $\eta = g/\omega_{TO}$	0.254	0.260	0.261	0.255

FWHM, full-width at half-maximum.

words, the classical approach can be used to compute the polaritonic branches exactly when the system enters into the USC regime. The same behaviour is valid for an arbitrary number of vibrational modes in the polar material (Supplementary Sections 8 and 10).

Experimental verification of dispersion and USC. We can therefore analyse the dependence of the ENZ resonant frequencies on the inner coaxial diameter using equation (5) (Fig. 3c–f). As ω_p is independent of the hole shape and size, the ENZ resonances in this strong-coupling condition depend only on the bare ENZ frequency, $\omega_{ENZ}(D)$. This bare ENZ frequency, in turn, is obtained from the upper polariton branch (Supplementary Section 12). This procedure is followed because the lower polariton is more affected by additional vibrational resonances that have not been considered in this simple analysis.

For each gap size, we estimate the coupling strength g as half the frequency difference between the upper and lower polariton branches when $\omega_{ENZ}(D) = \omega_{TO}$. Results are summarized in Fig. 3b and Table 1. Since the SiO_2 layer is added to our coaxial nanocavity during the fabrication process, it is not trivial to experimentally measure the bare ENZ resonance (that is, to measure the transmission of the cavity with an empty gap). Instead, we measure the linewidth of a bare ENZ resonance at a higher frequency, where it is uncoupled from the SiO_2 phonons. As shown in Table 1, all cavities exhibit modal splittings that are larger than the average of the linewidths of the bare cavity resonances and of the TO phonon ($2g/\gamma_{avg} > 1$). This indicates that the system is in the strong-coupling regime.

Moreover, the normalized coupling strength $\eta = g/\omega_{TO} > 0.25$, regardless of gap width, indicates that the systems are also in the USC regime[19]. For a single dipole emitter in a cavity of volume V, $g \propto 1/\sqrt{V}$. However, for collective coupling, as in our system, $g \propto \sqrt{N/V}$, where N is the number of dipoles coherently coupled to the cavity mode. Thus, g depends only on the density of molecules, N/V, and is independent of the coaxial gap width (Supplementary Section 3).

Conclusions

We have constructed wafer-scale resonant coaxial nanocavities and achieved USC between the ENZ mode of the cavities and SiO_2 phonons with a normalized coupling strength greater than 0.25. The large magnitude of the splitting we observe—wider than the Reststrahlen band—shows that the coupling strength is truly within the USC regime, and is not the manifestation of absorption induced within the forbidden band. To further elucidate this point, we also presented a theoretical framework (both classical and quantum mechanical) that quantitatively explains the data, and which can be applied to similar USC involving homogeneous materials, waveguides and resonant cavities.

The ENZ nanocavities can be filled with a variety of vibrationally active materials, thus enabling USC to be realized throughout the MIR, far-IR and terahertz spectral ranges. Furthermore, since single-nanometre-thick phononic films separate the core and cladding electrodes in each coaxial nanocavity, the platform provides a route to combine electron tunnelling with vibrational USC and EOT, which should enable observation of ground-state electroluminescence[46] and the dynamic Casimir effect[22,23]. The ability to reach the USC regime in mass-produced ENZ cavities with ultrasmall gap volumes ($\approx \lambda^3/10^7$) can also open up new avenues to explore quantum nonlinear optical processes[47], multiphoton effects, higher-order nonlinear effects and single-photon excitation of multiple atoms[48], which may lead to novel applications in quantum sensing, spectroscopy, optoelectronic devices and frequency conversion[49].

Online content

Any methods, additional references, Nature Research reporting summaries, source data, extended data, supplementary information, acknowledgements, peer review information; details of author contributions and competing interests; and statements of data and code availability are available at https://doi.org/10.1038/s41566-020-00731-5.

Received: 30 April 2020; Accepted: 26 October 2020;
Published online: 07 December 2020

References

1. Törmä, P. & Barnes, W. L. Strong coupling between surface plasmon polaritons and emitters: a review. *Rep. Prog. Phys.* **78**, 013901 (2015).
2. Ebbesen, T. W. Hybrid light-matter states in a molecular and material science perspective. *Acc. Chem. Res.* **49**, 2403–2412 (2016).
3. Pelton, M. Modified spontaneous emission in nanophotonic structures. *Nat. Photon.* **9**, 427–435 (2015).
4. Luk'yanchuk, B. et al. The Fano resonance in plasmonic nanostructures and metamaterials. *Nat. Mater.* **9**, 707–715 (2010).
5. Neubrech, F. et al. Resonant plasmonic and vibrational coupling in a tailored nanoantenna for infrared detection. *Phys. Rev. Lett.* **101**, 157403 (2008).
6. Yoshie, T. et al. Vacuum Rabi splitting with a single quantum dot in a photonic crystal nanocavity. *Nature* **432**, 200–203 (2004).
7. Reithmaier, J. P. et al. Strong coupling in a single quantum dot-semiconductor microcavity system. *Nature* **432**, 197–200 (2004).
8. Aoki, T. et al. Observation of strong coupling between one atom and a monolithic microresonator. *Nature* **443**, 671–674 (2006).
9. Liu, X. et al. Strong light–matter coupling in two-dimensional atomic crystals. *Nat. Photon.* **9**, 30–34 (2015).
10. Benz, F. et al. Single-molecule optomechanics in 'picocavities'. *Science* **354**, 726–729 (2016).
11. Santhosh, K., Bitton, O., Chuntonov, L. & Haran, G. Vacuum Rabi splitting in a plasmonic cavity at the single quantum emitter limit. *Nat. Commun.* **7**, 11823 (2016).
12. Runnerstrom, E. L. et al. Polaritonic hybrid-epsilon-near-zero modes: beating the plasmonic confinement vs propagation-length trade-off with doped cadmium oxide bilayers. *Nano Lett.* **19**, 948–957 (2018).
13. Leng, H., Szychowski, B., Daniel, M.-C. & Pelton, M. Strong coupling and induced transparency at room temperature with single quantum dots and gap plasmons. *Nat. Commun.* **9**, 4012 (2018).
14. Park, K.-D. et al. Tip-enhanced strong coupling spectroscopy, imaging, and control of a single quantum emitter. *Sci. Adv.* **5**, eaav5931 (2019).
15. Schoelkopf, R. J. & Girvin, S. M. Wiring up quantum systems. *Nature* **451**, 664–669 (2008).
16. Dunkelberger, A., Spann, B., Fears, K., Simpkins, B. & Owrutsky, J. Modified relaxation dynamics and coherent energy exchange in coupled vibration-cavity polaritons. *Nat. Commun.* **7**, 13504 (2016).
17. Munkhbat, B., Wersäll, M., Baranov, D. G., Antosiewicz, T. J. & Shegai, T. Suppression of photo-oxidation of organic chromophores by strong coupling to plasmonic nanoantennas. *Sci. Adv.* **4**, eaas9552 (2018).
18. Thomas, A. et al. Tilting a ground-state reactivity landscape by vibrational strong coupling. *Science* **363**, 615–619 (2019).
19. Kockum, A. F., Miranowicz, A., Liberato, S. D., Savasta, S. & Nori, F. Ultrastrong coupling between light and matter. *Nat. Rev. Phys.* **1**, 19–40 (2019).
20. Forn-Díaz, P., Lamata, L., Rico, E., Kono, J. & Solano, E. Ultrastrong coupling regimes of light-matter interaction. *Rev. Mod. Phys.* **91**, 025005 (2019).
21. Romero, G., Ballester, D., Wang, Y. M., Scarani, V. & Solano, E. Ultrafast quantum gates in circuit QED. *Phys. Rev. Lett.* **108**, 120501 (2012).

22. Johansson, J. R., Johansson, G., Wilson, C. M. & Nori, F. Dynamical Casimir effect in a superconducting coplanar waveguide. *Phys. Rev. Lett.* **103**, 147003 (2009).
23. Wilson, C. M. et al. Observation of the dynamical Casimir effect in a superconducting circuit. *Nature* **479**, 376–379 (2011).
24. Schwartz, T., Hutchison, J. A., Genet, C. & Ebbesen, T. W. Reversible switching of ultrastrong light-molecule coupling. *Phys. Rev. Lett.* **106**, 196405 (2011).
25. Niemczyk, T. et al. Circuit quantum electrodynamics in the ultrastrong-coupling regime. *Nat. Phys.* **6**, 772–776 (2010).
26. Jouy, P. et al. Transition from strong to ultrastrong coupling regime in mid-infrared metal-dielectric-metal cavities. *Appl. Phys. Lett.* **98**, 231114 (2011).
27. George, J. et al. Multiple Rabi splittings under ultrastrong vibrational coupling. *Phys. Rev. Lett.* **117**, 153601 (2016).
28. Scalari, G. et al. Ultrastrong coupling of the cyclotron transition of a 2D electron gas to a THz metamaterial. *Science* **335**, 1323–1326 (2012).
29. Shelton, D. J. et al. Strong coupling between nanoscale metamaterials and phonons. *Nano Lett.* **11**, 2104–2108 (2011).
30. Autore, M. et al. Boron nitride nanoresonators for phonon-enhanced molecular vibrational spectroscopy at the strong coupling limit. *Light Sci. Appl.* **7**, 17172 (2018).
31. Lather, J., Bhatt, P., Thomas, A., Ebbesen, T. W. & George, J. Cavity catalysis by cooperative vibrational strong coupling of reactant and solvent molecules. *Angew. Chem. Int. Ed.* **58**, 10635–10638 (2019).
32. Jin, X. et al. Reshaping the phonon energy landscape of nanocrystals inside a terahertz plasmonic nanocavity. *Nat. Commun.* **9**, 763 (2018).
33. Muller, E. A. et al. Nanoimaging and control of molecular vibrations through electromagnetically induced scattering reaching the strong coupling regime. *ACS Photonics* **5**, 3594–3600 (2018).
34. Baida, F. I., Belkhir, A., Labeke, D. V. & Lamrous, O. Subwavelength metallic coaxial waveguides in the optical range: role of the plasmonic modes. *Phys. Rev. B* **74**, 205419 (2006).
35. Alù, A. & Engheta, N. Light squeezing through arbitrarily shaped plasmonic channels and sharp bends. *Phys. Rev. B* **78**, 035440 (2008).
36. Yoo, D. et al. High-throughput fabrication of resonant metamaterials with ultrasmall coaxial apertures via atomic layer lithography. *Nano Lett.* **16**, 2040–2046 (2016).
37. Liberal, I. & Engheta, N. Near-zero refractive index photonics. *Nat. Photon.* **11**, 149–158 (2017).
38. Lindquist, N. C., Nagpal, P., McPeak, K. M., Norris, D. J. & Oh, S.-H. Engineering metallic nanostructures for plasmonics and nanophotonics. *Rep. Prog. Phys.* **75**, 036501 (2012).
39. Garcia-Vidal, F. J., Martin-Moreno, L., Ebbesen, T. W. & Kuipers, L. Light passing through subwavelength apertures. *Rev. Mod. Phys.* **82**, 729–787 (2010).
40. Born, M. & Huang, K. *Dynamical Theory of Crystal Lattices* (Oxford Univ. Press, 1988).
41. Hopfield, J. J. Theory of the contribution of excitons to the complex dielectric constant of crystals. *Phys. Rev.* **112**, 1555–1567 (1958).
42. Quattropani, A., Andreani, L. C. & Bassani, F. Quantum theory of polaritons with spatial dispersion: exact solutions. *Il Nuovo Cimento D* **7**, 55–69 (1986).
43. Ciuti, C., Bastard, G. & Carusotto, I. Quantum vacuum properties of the intersubband cavity polariton field. *Phys. Rev. B* **72**, 115303 (2005).
44. Todorov, Y. & Sirtori, C. Intersubband polaritons in the electrical dipole gauge. *Phys. Rev. B* **85**, 045304 (2012).
45. Kéna-Cohen, S., Maier, S. A. & Bradley, D. D. C. Ultrastrongly coupled exciton-polaritons in metal-clad organic semiconductor microcavities. *Adv. Opt. Mater.* **1**, 827–833 (2013).
46. Cirio, M., De Liberato, S., Lambert, N. & Nori, F. Ground state electroluminescence. *Phys. Rev. Lett.* **116**, 113601 (2016).
47. Kockum, A. F., Miranowicz, A., Macrì, V., Savasta, S. & Nori, F. Deterministic quantum nonlinear optics with single atoms and virtual photons. *Phys. Rev. A* **95**, 063849 (2017).
48. Garziano, L. et al. One photon can simultaneously excite two or more atoms. *Phys. Rev. Lett.* **117**, 043601 (2016).
49. Kockum, A. F., Macrì, V., Garziano, L., Savasta, S. & Nori, F. Frequency conversion in ultrastrong cavity QED. *Sci. Rep.* **7**, 5313 (2017).
50. Kischkat, J. et al. Mid-infrared optical properties of thin films of aluminum oxide, titanium dioxide, silicon dioxide, aluminum nitride, and silicon nitride. *Appl. Opt.* **51**, 6789–6898 (2012).

Methods

Device fabrication. After pre-cleaning and pre-baking steps (200 °C for 3 min), an undoped, double-side-polished 4-inch (100) Si wafer (University Wafer, Inc.) was spin-coated with AZ MiR 701 photoresist for 45 s at 5,000 r.p.m., followed by baking at 90 °C for 90 s. The patterns of hexagonal hole arrays with 24 different diameters from 430 nm to 1,120 nm were transferred onto the Si wafer by photolithography (Canon 2500 i3 stepper) with a dose of 150 mJ cm^{-2}, followed by a post-exposure bake at 110 °C and development with AZ 300MIF developer for 60 s. Hexagonal Au disk arrays were created on the Si wafer via directional evaporation of 3-nm-thick Ti and 150-nm-thick Au films (CHA, SEC 600), followed by liftoff using AZ Kwik Strip. After oxygen plasma cleaning (STS, 320PC) at 100 W for 30 s to remove photoresist residue, the Au disk arrays were coated conformally with a thin SiO_2 film using ALD (Cambridge Nano Tech Inc., Savannah) at a typical deposition rate of 1.2 Å per cycle. Atomic layer deposition was performed using ozone precursor and water vapour at 180 °C. After conformal sputtering of 3 nm Ti and 400 nm Au (AJA, ATC 2200), the top surface of 400-nm-thick Au-deposited disk patterns was planarized by glancing-angle ion milling using a 240 mA Ar^+ ion beam incident at 5° from the horizontal plane (Intlvac, Nanoquest) until the top entrance of the coaxial nanocavities was exposed.

Data availability

The data that support the plots within this paper and other findings of this study are available from the corresponding authors upon reasonable request.

Acknowledgements

We thank T. W. Ebbesen for helpful comments. This research was supported by grants from the US National Science Foundation (ECCS 1809240 to D.Y., D.A.M., S.-H.O.; ECCS 1809723 to I.-H.L., S.-H.O.) and the Samsung Global Research Outreach (GRO) Program (to S.-H.O.). F.d.L.-P. and L.M.-M. acknowledge financial support from the Spanish Ministry of Economy and Competitivity through projects MAT2017-88358-C3-1-R and MAT2017-88358-C3-2-R and the Aragón Government project Q-MAD. M.P. acknowledges support from the US National Science Foundation (NSF DMR-1905135). M.B.R. acknowledges funding from the US National Science Foundation (NSF CHE-1709822). J.D.C. was supported by the Office of Naval Research Grant N00014-18-12107. S.-H.O. further acknowledges support from the Sanford P. Bordeau Chair in Electrical Engineering at the University of Minnesota.

Author contributions

D.Y. and S.-H.O. conceived the project and designed experiments. D.Y. performed device design, fabrication and measurements. F.d.L.-P. and L.M.-M. developed theories and performed numerical calculations. D.A.M. and I.-H.L. performed computer simulations. D.Y., F.d.L.-P., M.P., D.A.M., I.-H.L., M.B.R., J.D.C., L.M.-M. and S.-H.O. analysed the results. All authors contributed to interpretation of the results and wrote the paper together.

Competing interests

The authors declare no competing interests.

Additional information

Supplementary information is available for this paper at https://doi.org/10.1038/s41566-020-00731-5.

Correspondence and requests for materials should be addressed to L.M.-M. or S.-H.O.